Heliyon 10 (2024) e25518

Contents lists available at ScienceDirect

Heliyon

journal homepage: www.cell.com/heliyon

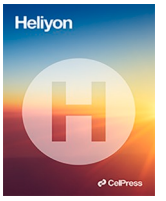

Research article

Structural determination, characterization and computational studies of doped semiconductors base silicon phthalocyanine dihydroxide and dienynoic acids

María Elena Sánchez Vergara [a,*], Emilio I. Sandoval Plata [a], Ricardo Ballinas Indili [b], Roberto Salcedo [c], Cecilio Álvarez Toledano [b]

[a] *Facultad de Ingeniería, Universidad Anáhuac México, Avenida Universidad Anáhuac 46, Col. Lomas Anáhuac, Huixquilucan, 52786, Estado de México, Mexico*

[b] *Instituto de Química, Universidad Nacional Autónoma de México, Circuito Exterior s/n. C.U., Delegación Coyoacán, C.P. 04510, Ciudad de México, Mexico*

[c] *Instituto de Investigaciones en Materiales, Universidad Nacional Autónoma de México, Circuito Exterior s/n, Ciudad Universitaria, Coyoacán, 04510, Ciudad de México, Mexico*

A R T I C L E I N F O

Keywords:
Silicon phthalocyanine dihydroxide
Dienynoic acid
DFT calculations
Semiconductor film
Optoelectronic characterization

A B S T R A C T

The chemical doping of silicon phthalocyanine dihydroxide ($SiPc(OH)_2$), with (2E, 4Z)-5, 7-diphenylhepta-2, 4-dien-6-ynoic acids (DAc) with electron-withdrawing (BrDAc) and electron-donating (MeODAc) substituents is the main purpose of this work. Theoretical calculations were carried out on Gaussian16 software, with geometrical optimization of all involved species, and obtention of the highest occupied molecule orbital (HOMO), lowest unoccupied molecular orbital (LUMO), and the respective energy gaps. The theoretical calculations show two hydrogen bridge formations: the first one as a peripheral interaction between the terminal oxygen atoms from the acid unit and hydrogen atoms from the phthalocyanine aromatic rings. The second one as the interaction at the nitrogen atoms of the phthalocyanine, which are compelled to form a new flat plane far from the original flat phthalocyanine deck. These organic semiconductors were deposited as thin films and characterized by IR spectroscopy, atomic force microscopy (AFM), and the optical parameters were gathered from UV–Vis studies. The indirect and direct optical band gap, the onset gap and the Urbach energy were obtained. In order to compare the effect of the acids as dopants of the silicon phthalocyanine, the $SiPc(OH)_2$-DAc films were electrically characterized. The $SiPc(OH)_2$-DAc films exhibit an ambipolar electrical behavior, which is influenced by the incidence of different lighting conditions at voltages above 0.3V. The glass/ITO/$SiPc(OH)_2$-MeODAc/Ag reaches a maximum current of 5.68×10^{-5} A for natural light condition, while the glass/ITO/$SiPc(OH)_2$-BrDAc/Ag, reaches a maximum current of 9.21×10^{-9} A for white illumination condition.

* Corresponding author.
E-mail addresses: elena.sanchez@anahuac.mx (M.E. Sánchez Vergara), esandoval@anahuac.mx (E.I. Sandoval Plata), ricardoballinas1989@gmail.com (R. Ballinas Indili), salcevitch@gmail.com (R. Salcedo), cecilio@unam.mx (C. Álvarez Toledano).

https://doi.org/10.1016/j.heliyon.2024.e25518
Received 23 August 2023; Received in revised form 24 January 2024; Accepted 29 January 2024
Available online 2 February 2024

1. Introduction

Intensive research has been carried out in recent years in the field of organic semiconductors, mainly focused on their application in electronic, optoelectronic, and photovoltaic devices. Organic semiconductors have not yet reached the prominence of inorganic semiconductors such as silicon, since the latter exhibit greater efficiencies and higher values of charge mobilities in their devices. However, their easy processing, the possibility of coating flexible surfaces, and their low cost make organic semiconductors attractive to be extensively used in electronics. In contrast with inorganic materials, the optical and electrical properties of organic semiconductors can be mainly attributed to their chemical structure, as they do not require an ordered crystal formation [1]. Organic semiconductors, on the other hand, need a conjugated structure to be able to take part in charge transport effectively [2,3]. The nature of their π orbitals allows the stabilization of the electronic charge by resonant effect and facilitates intermolecular interactions by the overlapping of its orbitals, which favors charge transport. Therefore, the adequate choice of an organic base structure plays an influential role in the design of novel organic semiconductor materials. Another advantage of these semiconductors is the ease of manipulating their properties by functionalization or introduction of substituents during their chemical doping.

Inside the organic semiconductor field, phthalocyanines (Pcs) serve as organic conjugated molecules that can be doped to be applied in optoelectronics and photovoltaics devices [4]. Pcs are also known as tetrabenzotetraazaporphyrins, as they are synthetic porphyrin analogs differing just on the four benzo-subunits and bonding nitrogen at the meso positions [5]. Pcs exhibit aromaticity due to their planar 18 π-electron array, which also encourages self-aggregation onto ordered molecular stacks. They are composed by four imine-bridged isoindole subunits on a ring formation with a central cavity similar to porphyrins, which can accommodate about 70 different elemental ions [5,6]. The incorporation of usually one +2 or two +1 metal cations into the cavity through oxidation of the Pc^{2-} dianion, or by metal ion inclusion during the macrocycle synthetic route, gives rise to the Metallo-phthalocyanine derivatives (MPcs) [5]. MPcs exhibit many interesting properties and applications in numerous fields, such as industrial colorants, optoelectronics, photovoltaics, organic semiconductors, and medicinal chemistry, amongst others, aided by their chemical flexibility for structural modification and adjustment of these properties [7–9]. Such properties are mainly attributed to the highly ordered intermolecular planar face π–π stacking interactions such as dimerization or aggregation in between adjacent MPc molecules, which delocalize electrons along the central column axis π–π orbital overlaps. This leads to fluorescence quenching and a broad absorption Q-band of 650–670 nm in the visible spectrum, which provides MPcs their characteristic blue-shifted hues even on very dilute solutions [7,8]. Nevertheless, some MPc derivatives of interest are not able to form aggregates on account of structural features such as axial or bulky peripheral substitutions, which avoids a proper π–π orbital overlapping, exhibiting sharper peaks of UV–vis absorption and emission, as well as more intensive photoluminescence, since there is no formation of a conduction band [7,8].

An attractive group of Pcs are Si(IV) incorporated MPcs, due to the low toxicity and elemental abundance of silicon, in addition to their low energy gap (~1.7 eV) [10]. Silicon phthalocyanine compounds (SiPcs) have been extensively studied for their intense absorption levels in the visible portion of the spectrum [11,12]. Unlike most MPcs and other core-substituted Pcs, silicon phthalocyanines (SiPcs) bring additional possibilities, as their hexacoordinated core-substituent Si(IV) ion allows the two additional axial substitution positions beyond only the peripheral ring α and β *Pc* positions, in addition to the great Si–N bond stability [9,13]. Substituents at these axial positions tend to disturb planarity, therefore reducing aggregation and hydrophobicity and thus diminishing the π–π stacking and improving photophysical properties [7,9]. The axial ligands can be employed as pivotal handles for fine regulation of SiPcs characteristics as desired and give control over the optoelectrical properties of the SiPcs characteristics as desired and give control over the optoelectrical properties of the material [9,14]. For example, R_2-SiPc where R can be siloxide or aryloxide ligands have been applied as fluorophores and chromophores in dye-sensitized solar cells and organic light emitting diodes [10]. Also, some studied SiPc derivatives have been PhCOO-SiPc, NpCOO-SiPc, AnCOO-SiPc and Cl_2-SiPc as components of organic thin-film transistors [14]. Besides, SiPcs with axial oxygen-terminated ligands (siloxide, aryloxide, and carboxylate) have been applied as photosensitizing agents in photodynamic therapy due to their photophysical characteristics, their bio-inertness and chemical stability [10,15]. On the other hand, different fluorophenoxy substituents in SiPc, were employed as electron donors and acceptors in organic photovoltaic devices [15]. The insertion of electron-withdrawing and -donating moieties can modify the optoelectronic behaviour of SiPcs [8,9,15,16].

The structural fine-tuning of SiPcs is mainly achieved by means of two precursors: $SiPcCl_2$ and $SiPc(OH)_2$, this latter synthesized from the first [13,17]. With this in mind, this work proposes the study of $SiPc(OH)_2$ as an active layer in which radiation emission takes place after the encounter of holes and electrons, in optoelectronic devices. $SiPc(OH)_2$ has been little studied as an organic semiconductor in an active layer, and its structure with symmetrical ligands can display interesting optical and electronic properties. For the manufacture of the active layer, an innovative dopant of $SiPc(OH)_2$ which behaves as a p-type semiconductor [18] is proposed: the (2E, 4Z) dienynoic acids that show an n-type semiconductor behaviour. Doping is expected to improve the efficiency of the device by modifying the conductive properties of phthalocyanine and allowing more efficient charge transport in $SiPc(OH)_2$-DAc films. The physical properties of both (2E, 4Z) dienynoic acids are similar, with a reported crystalline structure and X-ray diffraction analysis only for Br-DAc [19]. The structural arrangement exhibits the (E,Z) double bond conformation in the formation of dienynoic acid, the (2E, 4Z) dienynoic acids have high thermal stability. A push-pull system is allowed by the inclusion of bromide, where the carbonyl pulls, and the triple bond donates electronic density to partially compensate for electronic dislocation. Since halogens have the property of being an electron-donating group by resonant effect and an electron-withdrawing group by induction, they are capable of producing a molecule with a semiconductor behaviour [19]. The importance of the present work is focused on three relevant aspects, the study of (i) the effect of the acid as a dopant, in the $SiPc(OH)_2$, (ii) the deposit of $SiPc(OH)_2$-DAc films with optical and electrical properties, and (iii) the complementation of the obtained experimental results, with the theoretical calculations obtained employing Density Functional Theory (DFT), which will allow to analyse the interaction between the $SiPc(OH)_2$ and the acids, as well as the obtaining of the HOMO, LUMO, and the band gaps of these organic semiconductors.

2. Experimental

Silicon phthalocyanine dihydroxide ($SiPc(OH)_2$: $C_{32}H_{18}N_8O_2Si$) was acquired from Sigma-Aldrich and required no additional purification. The (2E, 4Z)-5, 7-diphenylhepta-2, 4-dien-6-ynoic acids (Br-DAc and MeO-DAc) were obtained as specified by previously detailed procedures by some of the authors of this work [19]. Chemical doping was carried out on two mixtures of $SiPc(OH)_2$ and a DAc (see Fig. 1), prepared under the mass ratio of 2:1 respectively in the common solvent MeOH. The synthesis was performed in a heated Monowave 50 reactor under controlled time, temperature, and pressure; employed with a borosilicate glass vial and shut by a cover with a temperature sensor and 20 bar of integrated pressure. The reactions were maintained for 30 min before system temperature and pressure were brought back to normal atmospheric conditions. The products of the reactions were washed with MeOH and then dried under vacuum conditions to obtain the doped semiconductors as powders. As a preliminary discernment of the doped semiconductors from their doping reagents, chemical characterization was carried out by IR spectroscopy with a Nicolet iS5-FTIR spectrometer in spectroscopic grade KBr pellets on wavelengths of 4000 to 400 cm^{-1}. Additionally, an optical absorbance analysis for the doped semiconductors, was conducted on a UV–vis 300 Unicam spectrophotometer in 10^{-5} M MeOH solutions.

For further optical and electrical characterization of the doped semiconductors ($SiPc(OH)_2$-DAc) as well as undoped $SiPc(OH)_2$ in solid state, thin films were deposited via high-vacuum sublimation method onto four substrates each: high-resistivity monocrystalline n-type silicon wafer, Corning glass slide, indium tin oxide ($In_2O_3{\cdot}(SnO_2)_x$) coated polyethylene terephthalate film (PET-ITO), and indium tin oxide coated glass slide (glass-ITO). For greater film adherence and performance, Si substrates were cleansed; with a "p" (10 mL HF, 15 mL HNO_3, 300 mL H_2O) solution. Likewise, glass-ITO and Corning glass cleansing were performed by sequential ultrasonic processes under chloroform, MeOH, and acetone solvents, followed by vacuum drying. Sublimation was conducted inside a high vacuum chamber, composed by a mechanical pump for a first vacuum of 10^{-3} Torr and a turbo-molecular pump for the final vacuum of 10^{-6} Torr. Undoped $SiPc(OH)_2$ and $SiPc(OH)_2$-DAc powders were individually placed in a molybdenum crucible inside the chamber and heated to a gaseous state phase change, to finally be deposited onto the room temperature substrate slides upon contact, with deposition rates of 3.7, 15.4, and 8.3, Å/s for $SiPc(OH)_2$, $SiPc(OH)_2$-BrDAc, and $SiPc(OH)_2$-MeODAc respectively. The thicknesses of the films were recorded by a high-resolution quartz-crystal microbalance monitor connected to a thickness sensor, resulting in final thicknesses of 84, 192, and 159 Å respectively. To confirm the absence of chemical degradation during the sublimation process, the films coated on n-type Si wafer was analysed by IR spectroscopy. Topographical characteristics were investigated with a Nano AFM atomic force microscope using a Ntegra platform for the films deposited on the Si wafer substrate. UV–Vis absorbance and transmittance spectra of $SiPc(OH)_2$-DAc films on Corning glass substrates at 190–1100 nm wavelengths, employing an UV–vis 300 Unicam spectrophotometer as a means to calculate optical band gaps. For electrical-behaviour characterization of $SiPc(OH)_2$-DAc films, simple devices were prepared according to the scheme in Fig. 1, the ITO was utilized as an anode, and the Ag onto the semiconductor film acted as cathode. The silver cathodes were located in two different zones of each film, in order to verify the current-voltage measurements. The glass/ITO/$SiPc(OH)_2$-DAc/Ag were measured by the four collinear-probe methods on a Keithley 4200-SCS-PK1 voltage source with an auto-ranging pico-ammeter, under controlled lighting by a Next Robotics controller circuit. The lighting conditions were given using LEDs with the following characteristics: UV (2.70 eV), blue (2.64 eV), green (2.34 eV), yellow (2.14 eV), orange (2.0 eV), red (1.77 eV), in addition to ambient light and darkness.

3. Computational method

Computational calculations were carried out on several of the molecules belonging to this study. A hybrid method which combines the Becke gradients correction [20] which performs the exchange with the Perdew and Wang subroutines for correlation [21] (i.e. B3PW91) was chosen. This hardware is found in the Gaussian package which was used [22]. The method M06 [23] which has demonstrated its utility for special cases [24] was applied to obtain the molecular orbitals and the simulation of spectra. In all cases the basis 6–31g** was used and also frequency calculations were carried out in order to assure the minimum of energy in the potential energy surface.

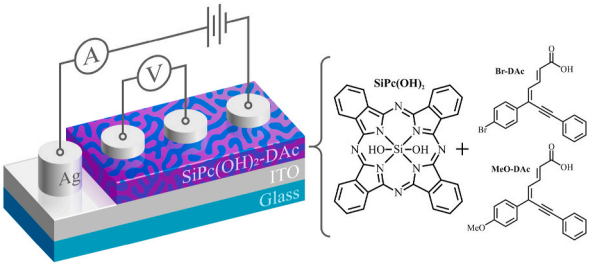

Fig. 1. $SiPc(OH)_2$-DAc device for electrical characterization.

4. Results and discussión

4.1. Theoretical results

The interaction of $SiPc(OH)_2$ and DAc was theoretically studied in order to assess the type of semiconductor behavior that $SiPc(OH)_2$-DAc structures could demonstrate, in terms of their HOMO and LUMO. In devices such as diodes or solar cells, it is necessary to consider that the anode injects holes toward the HOMO of the organic semiconductor, whereas from the cathode, the electrons are injected toward its LUMO. Therefore, active layers with energetic values of their HOMO and LUMO orbitals are required, as aligned as possible with the electrode work function of the device. The analysis reported in this section is focused on the interaction of the phthalocyanine which bears OH- groups substituted on the central Si atom with both derivatives of the dienynoic acid, the one with the weak electro-donating substituent (BrDAc) and the one with strong electro-donating substituent (MeODAc). In both cases the formation of hydrogen bridges was identified, thus they were calculated using the Grimme software yielding the following results. There are two cases in where hydrogen bonds can be formed, in the first one there are peripheral influence between hydrogen atoms from the phthalocyanine aromatic rings and the terminal oxygen atoms from the acid units (Fig. 2a) or the bromine atom of BrDAc (Fig. 2b). The second one is the interaction of the nitrogen atoms of the phthalocyanine and terminal hydrogen atoms from the acid (Fig. 2c), which are compelled to form a new flat plane far from the original flat phthalocyanine deck or between the hydrogen from methoxy group MeODAc (Fig. 2d). All the possibilities are shown in Fig. 2 and the bond length values and energy of hydrogen bridges are shown in Table 1. These assembled hydrogen bonds play a very important role because they keep the structures of phthalocyanine and acid together and unaltered, this enhances the mobility of charge carriers, thanks to molecular stacking. Hydrogen bonding decreases the separation between $SiPc(OH)_2$ and acid originating interesting improvements such as greater charge transport, increased thin film-forming properties and higher white light emission efficiency [25]. These results are of importance because according to the literature [9], the acid is expected to interact with phthalocyanine at the axial hydroxides or at the phthalocyanine ring (α) and (β) positions. However, in this case, the $SiPc(OH)_2$-acid interactions take place at different sites, which will modify the optical behavior of the semiconductor phthalocyanine [9].

The energies of HOMO and LUMO have a remarkable role in electrical and photonic properties [26,27]. The HOMO-LUMO energetic interval or band gap in organic semiconductors, is consequence of intermolecular charge transfer from electron-donating

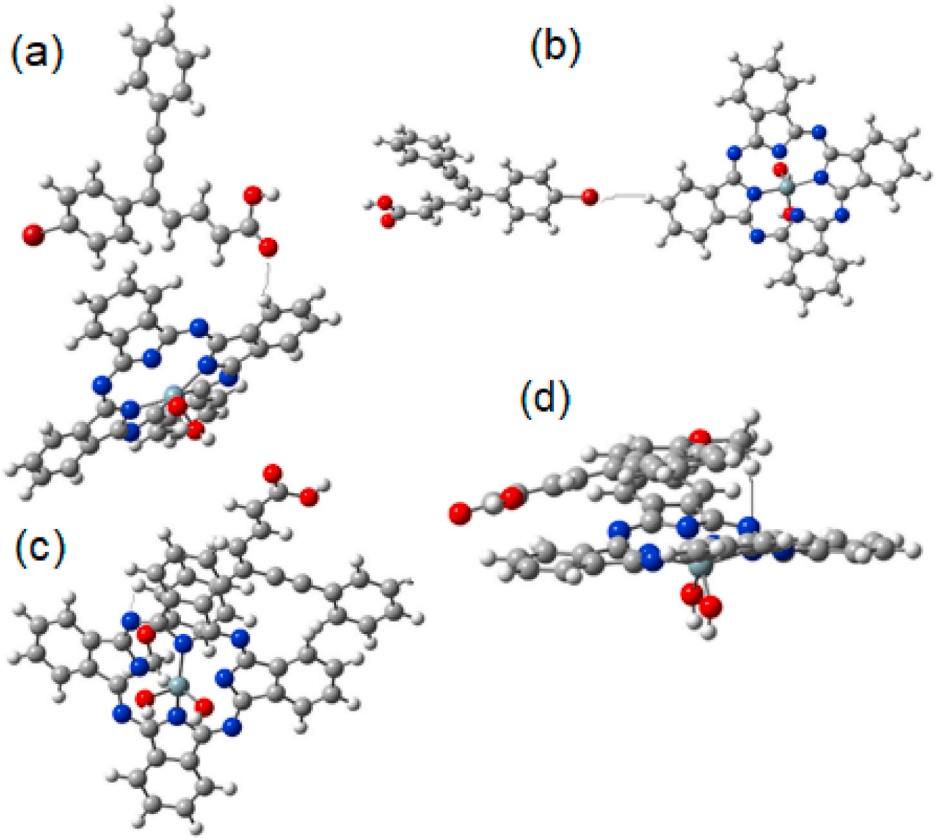

Fig. 2. Hydrogen bridges; (a) between terminal hydrogen from phthalocyanine and carboxylic oxygen of acid derivatives, (b) between terminal hydrogen from phthalocyanine and bromine atom of BrDAc, (c) between nitrogen atoms from phthalocyanine and terminal hydrogen atoms from acid analog and finally (d) between the hydrogen from methoxy group MeODAc and nitrogen from phthalocyanine.

Table 1
Bond length values and energy of hydrogen bridges for $SiPc(OH)_2$-DAc structures.

Molecule	Bond length (Å)	Energy (kcal/mol)
(a)	2.51	36.2
(b)	3.13	31.1
(c)	3.2	23.5*
(d)	2.85	30.7

towards electron-accepting groups [26]. The molecular orbitals HOMO, LUMO, and the band gap analysis indicate that the electronic behavior of the composed complexes emerges only from phthalocyanine. Table 2 shows the corresponding energy gap values in free molecules as well the formed complexes. If it is considered that the energy gap is related to the ability of electrons to jump from HOMO to LUMO, and if the band gap is smaller, then the semiconductor capacity of the material is greater, Table 2 shows that the precursors $SiPc(OH)_2$ and the (2E, 4Z) dienynoic acids have a higher energy gap than the doped structures $SiPc(OH)_2$-BrDAc and $SiPc(OH)_2$-MeODAc. This is indicative of increased charge transport in the doped phthalocyanine, which can be verified experimentally. It is noteworthy that the 2 eV energy gap obtained for the $SiPc(OH)_2$-DAc structures, sets them as semiconductor materials. It is also considerable that the obtained values for the HOMO, the LUMO and the band gap have the same order of magnitude as obtained by Pal et al. [10] for silicon phthalocyanine carboxylate esters and by Solgun et al. [26] for bis-(3,4-dimethoxyphenethoxy) axially substituted silicon phthalocyanine groups.

Regarding Fig. 3, the molecular orbital shapes suggest almost all the electronic flux is found on the plane of the phthalocyanine species. Fig. 3 shows two examples of the HOMO-LUMO set for two cases, the one of the $SiPc(OH)_2$-BrDAc (Fig. 3a), with lateral hydrogen bridge and the one of the methoxy derivative $SiPc(OH)_2$-MeODAc (Fig. 3b) with the surface interaction. Nevertheless; the decrease of the energy gap in the two doped species with respect to the energy gap of the pristine $SiPc(OH)_2$, evidences both the positive effect on the transport of charges of the hydrogen bond that links the phthalocyanine to the acid, and of the effect of this n-type electron donor dopant on the semiconductor structure. The transfer of electrons and the dissociation of the exciton between both compounds is ensured, since the energy level of the LUMO orbital of BrDAc acid, considered as the electron donor, is 0.3 eV above the LUMO orbital of phthalocyanine, and in the case of MeODAc acid is 0.9 eV above $SiPc(OH)_2$ [28]. There are additional factors such as polarity, which can alter the compound charge transport characteristics in a device. Fig. 3c–d shows the mapped electrostatic potential onto the electron densities of $SiPc(OH)_2$-DAc species. The red regions depict the electronegative poles and are defined as the electrophilic region, localized on the carboxylic region of the acid. On the other hand, the zones depicted in blue correspond to the most positive parts and constitute the nucleophilic region [28], which is located in one of the phthalocyanine rings. However, the experimental study is necessary to completely describe the distribution and transport of charges in $SiPc(OH)_2$-DAc semiconductors.

4.2. *Doping and characterization of $SiPc(OH)_2$-DAc*

Theoretical IR results (Fig. 4a and b), indicated the feasibility of conducting experimental doping of the semiconductors $SiPc(OH)_2$-DAc. Following the chemical doping, the main functional groups of the compounds were characterized via IR spectroscopy in order to verify if the doping of the phthalocyanine with the acids was properly carried out. The IR spectra performed in the KBr pellets (Fig. 4c and d) and those theoretically obtained were compared and concur well together; both are shown in Fig. 4. For the $SiPc(OH)_2$ the band present at 1612 ± 1 cm^{-1} corresponds to the C=C isoindole stretching [29–32], whereas the bands at 1122 ± 4 cm^{-1} and 910 ± 2 cm^{-1} are assigned to the in-plane and out of plane C–H bending deformations respectively [29–32]. The bands attributed to the in-plane stretching vibration of pyrrole are visible at 1330 ± 3 cm^{-1} for the phthalocyanine ring, and at 1164 ± 2, for the C–N in isoindole [29–32]. Also, the signal around 777 ± 1 cm^{-1} corresponds to the β-form in $SiPc(OH)_2$ [30,33]. This crystalline β-form generates an angle $\theta = 45.8°$ comprised between the axis of symmetry normal to the phthalocyanine plane, and an axis along the stacking direction of the phthalocyanine molecules [30,33]. Regarding the presence of the dienynoic acids BrDAc and MeODAc, the IR spectra of Fig. 4 and Table 3 demonstrate their characteristic signal, corresponding to the vibration of the C=O (1680 ± 2 cm^{-1}) [20]. The signals of COO–H, and the internal alkyne C≡C are absent from the calculated spectrum, however, the present phthalocyanine signals and the C=O signal of the DAc acids, indicate that the doping process was performed. The good accordance between experimental and theoretically obtained IR spectra evidences the viable approach that the calculations represent to this study.

In order to analyse electronic transitions within the $SiPc(OH)_2$-DAc semiconductors, a UV–vis spectroscopy study was conducted. Phthalocyanines are highly optically stable compounds, which absorb electromagnetic radiation from the visible spectrum portion. The $SiPc(OH)_2$ UV–vis spectrum of chromophore presents two bands, the *Q*-band correspondent to the red hues of the spectrum and the

Table 2
HOMO, LUMO, and Energy gap of $SiPc(OH)_2$-DAc and precursors.

Molecule	HOMO (eV)	LUMO (eV)	Energy gap (eV)
$SiPc(OH)_2$	−5.2	−2.9	2.3
BrDAc	−5.9	−2.6	3.3
MeODAc	−5.6	−2.0	3.6
$SiPc(OH)_2$-BrDAc	−4.95	−2.88	2.07
$SiPc(OH)_2$-MeODAc	−5.2	−3.2	2.0

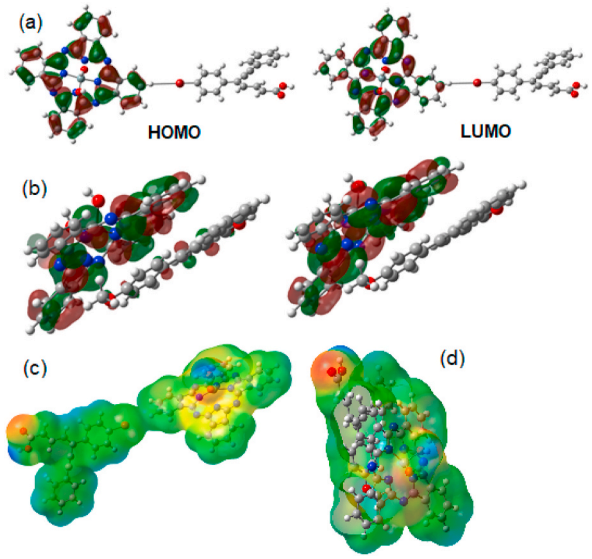

Fig. 3. Frontier HOMO and LUMO from the organic semiconductor (a) $SiPc(OH)_2$-BrDAc and (b) $SiPc(OH)_2$-MeODAc. Electrostatic potential mapped onto the electron densities of (c) $SiPc(OH)_2$-BrDAc and (d) $SiPc(OH)_2$-MeODAc from B3PW91/6-31G** calculations.

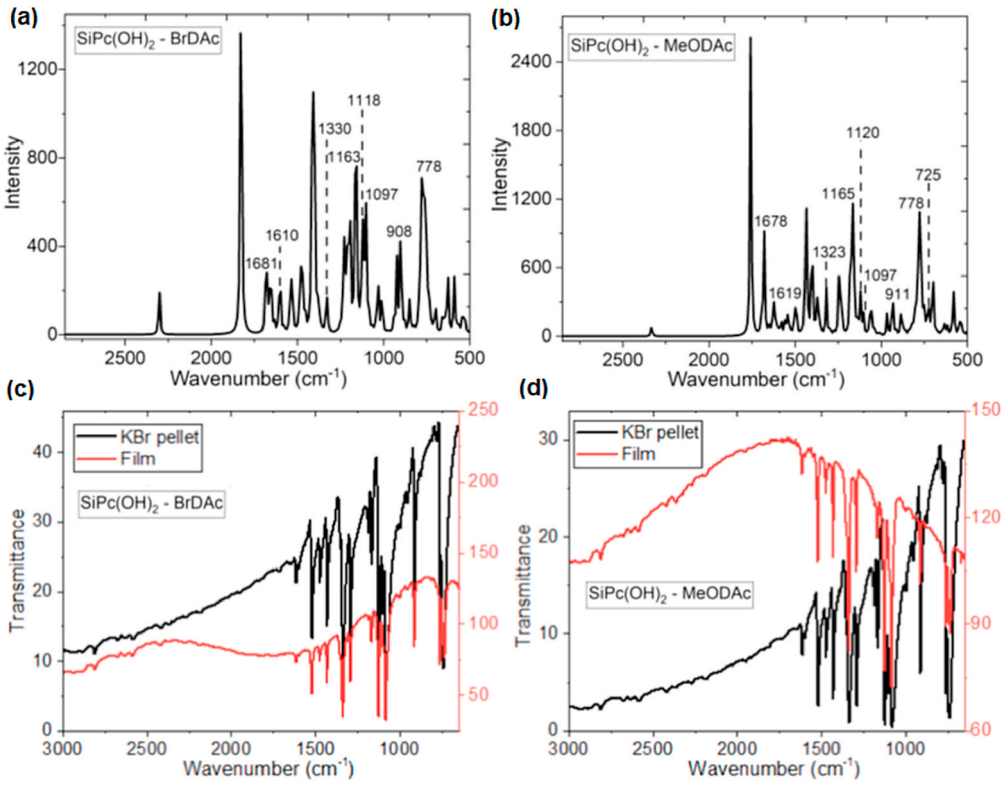

Fig. 4. (a, b) Calculated IR spectrums and (c, d) Experimental IR spectrums of $SiPc(OH)_2$-DAc in KBr pellet and films.

B-band in the near UV region [10,30], caused by its 18-π electrons conjugated aromatic cycle. The Q band is associated with π→π* HOMO-LUMO between orbitals of a_u and b_g symmetries [31,33–36], and the B band is caused by electronic π→π* related transitions of higher energy, from occupied orbitals of b_u and a_u symmetries less energetic than the LUMO [29,33–36]. According to the spectrum obtained in 10^{-5} M MeOH solution, shown in Fig. 5a, $SiPc(OH)_2$ presents the two characteristic bands, Q and B at 670 and 330 nm respectively. In other context; $SiPc(OH)_2$-BrDAc and $SiPc(OH)_2$-MeODAc spectra have much lower absorbance than for pristine SiPc

Table 3
Characteristic FT-IR bands for $SiPc(OH)_2$-DAc in KBr pellets and films.

Assignation	*$SiPc(OH)_2$ - BrDAc Pellet*	*$SiPc(OH)_2$ - BrDAc Film*	*$SiPc(OH)_2$ - MeODAc Pellet*	*$SiPc(OH)_2$ - MeODAc Film*
ν (CH) cm^{-1}	1122, 910	1124, 910	1123, 911	1126, 912
ν (C]C) cm^{-1}	1611	1613	1612	1611
ν (C–N) cm^{-1}	1163	1163	1163	1166
ν (C]N) cm^{-1}	1333	1333	1335	1336
β- form cm^{-1}	776	777	776	778
ν (COO–H) cm^{-1}	2933	2937	2970	2962
ν (C ^ C) cm^{-1}	2197	2199	2193	2192
ν (C]O) cm^{-1}	1682	1675	1681	1679

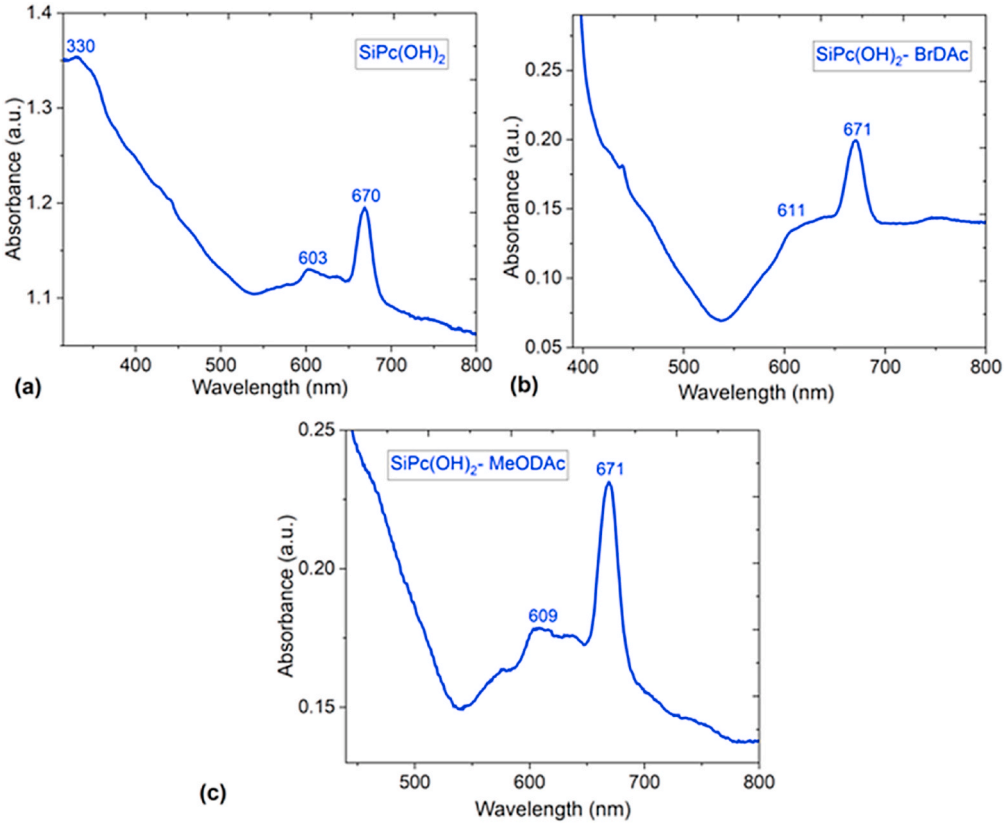

Fig. 5. UV–vis spectra of (a) $SiPc(OH)_2$, (b) $SiPc(OH)_2$-BrDAc and (c) $SiPc(OH)_2$-MeODAc in 10^{-5} M MeOH solutions.

$(OH)_2$. These spectra presents similarities with respect to the UV–vis spectrum reported by Vebber et al. [37] for silicon phthalocyanine ternary additives, the one reported by Honda et al. [38] for silicon naphthalocyanine bis(trihexylsilyl oxide), that reported by Grant et al. [39] for bis(tri-*n*-propylsilyl oxide) silicon phthalocyanine and that reported by Melville et al. [40] for bis(pentafluorophenoxy) silicon phthalocyanine and bis(2,4,6-trifluorophenoxy) silicon phthalocyaninde. However, in the $SiPc(OH)_2$-BrDAc (Fig. 5b) and $SiPc(OH)_2$-MeODAc (Fig. 5c) spectra, only the Q band is observed slightly bathochromically shifted. The shift towards longer wavelengths may be attributed to the strong electronic interactions between the acid and $SiPc(OH)_2$ [41], which reduces the aggregation and hence changes the absorption. Another important observation is that in a similar way in the doped semiconductors spectra, a vibronic band or the peak called shoulder at 606 ± 3 nm [41] is presented. In terms of UV–vis study, the acid dopant has a remarkable effect on the optical properties of the *Pc* ring, decreasing the overall absorbance in the doped semiconductors, red shifting the Q band, and inhibiting the presence of the B band. Finally, as seen in Fig. 5, the organic semiconductors exhibit non-aggregation behavior, which is relevant for its potential use as a photosensor.

4.3. Deposition and characterization of semiconductor films

With the aim of analyzing its solid-state properties, $SiPc(OH)_2$-BrDAc and (c) $SiPc(OH)_2$-MeODAc can be deposited in thin films.

After carrying out the deposition of the $SiPc(OH)_2$-DAc films, IR spectroscopy was performed to (i) determine if high vacuum sublimation is a useful approach for the deposition of thin films, and whether or not there is a decomposition of the compounds that constitute the films and (ii) knowing the α or β crystalline form of $SiPc(OH)_2$ after deposition. When comparing the IR spectra of the doped semiconductors on the KBr pellet and on the film (Fig. 4c and d), similar signals are observed. The IR spectroscopy results for the deposited films, which are also summarized in Table 3, reveal that $SiPc(OH)_2$-DAc deposited by evaporation under high vacuum, are thermally stable and do not undergo decomposition during their deposition process. On the other hand, the IR spectrum presents the signal at $777 \pm 1\ cm^{-1}$, characteristic of the β-form of phthalocyanine [30,33]. The β-form exhibits an angle of 45.8° with respect to an axis *b*, along which the columns of molecular stacking are formed [42].

On the other hand, the surface of the films was topographically studied by means AFM, which, as seen in Fig. 6, demonstrate a very different appearance from each other. As the film deposition was conducted under the same conditions of vacuum, temperature, and type of substrates, the difference in their topography is a consequence of the type of substituent in the acid structure. The substituent influences the stacking process of the molecules, which also influences their rate of deposition. The $SiPc(OH)_2$-BrDAc film (see Fig. 6a) has a higher deposition rate (15.4 Å/s) than the $SiPc(OH)_2$-MeODAc film (see Fig. 6b) (8.3 Å/s), and its RMS (Root Mean Square) roughness is also higher: 22.66 nm against the RMS of 12.19 nm respectively. The $SiPc(OH)_2$-BrDAc film is deposited more quickly in preferential sites, which induces a greater formation of nuclei, which grow quickly and with no time to achieve an ordered arrangement. This is reflected in the higher roughness than that obtained in the $SiPc(OH)_2$-MeODAc film. It is to be expected that this last film exhibits better conditions of electric charge transport.

The films were also evaluated by UV–Vis spectroscopy, to determine their main optical parameters such as the transmittance, absorption coefficient, the photon's energy, the optical band gap, and the Urbach energy. Concerning the transmittance plotted in Fig. 7a, it is observed that the pristine phthalocyanine exhibits greater transparency than the doped films. This transmittance of about 65 % for wavelengths between 480 and 550 nm and 70 % for wavelengths greater than 770 nm is less than that reported for other phthalocyanines with axial ligands such as $TiPcCl_2$ [43] and $SnPcCl_2$ [32]. On the other hand, doped films have a maximum transmittance of 50 % for $SiPc(OH)_2$-MeODAc and 26 % for $SiPc(OH)_2$-BrDAc as a result of the presence of acids. These dopants favor the absorption in the films and significantly lower their transparency. Fig. 7b shows the absorbance spectrum for $SiPc(OH)_2$, $SiPc(OH)_2$-BrDAc and $SiPc(OH)_2$-MeODAc films. The phthalocyanine absorbance spectrum arisen from the orbital overlapping from the silicon atom and its 18 π-electron orbital system [44–46]. Additionally, for all the films the Q-band appears between 1.7 and 2.4 eV in the visible region. For the $SiPc(OH)_2$-MeODAc and $SiPc(OH)_2$-BrDAc films, the Q-band band consists of a shoulder referred to the π-π* phthalocyanine transition [45]. The B-band can be perceived in the UV region, at the photon energy range from 2.68 eV to 3.12 eV. According to El-Damhogi et al. [44] the B-band is ascribed to the π-π* transition and, a split in it has been described as the Davydov splitting (ΔB), equal to 0.22 eV for $SiPc(OH)_2$ film, 0.09 eV for $SiPc(OH)_2$-MeODAc film and 0.11 eV for $SiPc(OH)_2$-BrDAc film. The splitting depends on the angle dipole moment transitions and the lengths in between an interacting number of adjacent molecules [44,47]. Finally in the absorbance spectra is showed that when the $SiPc(OH)_2$-MeODAc and $SiPc(OH)_2$-BrDAc films are exposed to ultraviolet rays, the absorbance increased. Dieninoic acids MeODAc and BrDAc increase the absorbance of doped films, which can be reflected in a higher absorption coefficient (α).

The α of a solid characterizes the films on the intensity attenuation of the photon by traversed thickness. Regarding the absorption of $SiPc(OH)_2$-DAc films, its absorption coefficient (α) is experimentally obtained from equation (1):

$$\alpha = ln(T / d) \tag{1}$$

Where T is the transmittance, and whose spectra are presented in Fig. 7a, and d is the film thickness recorded in Table 4. Regarding the photon's energy ($h\nu$), h is Planck's constant, and ν is the frequency obtained from equation (2):

$$\nu = \frac{c}{\lambda} \tag{2}$$

Where λ is the UV–vis spectral wavelength, and c is the speed of light. The parameter α is presented graphed with respect to the $h\nu$ in Fig. 8a. The *Q*-band and *B*-band of phthalocyanine appear well differentiated and as expected, with a higher absorption coefficient for the $SiPc(OH)_2$-DAc films. A requirement for the appropriate performance of a film in an optoelectronic device is its absorption capacity as a minimum, which is related to electronic delocalization in its molecular structure. In this case, α is in the range $10^6\ cm^{-1}$, supporting its potential as an absorbent material for solar and optoelectronic applications [48].

In order to compare the experimental result with the theoretically calculated energy gap the optical band gap (E^{opt}) was evaluated

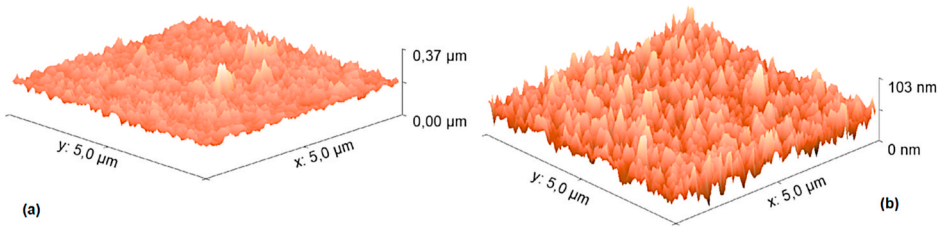

Fig. 6. AFM images of (a) $SiPc(OH)_2$-BrDAc and (b) $SiPc(OH)_2$-MeODAc films.

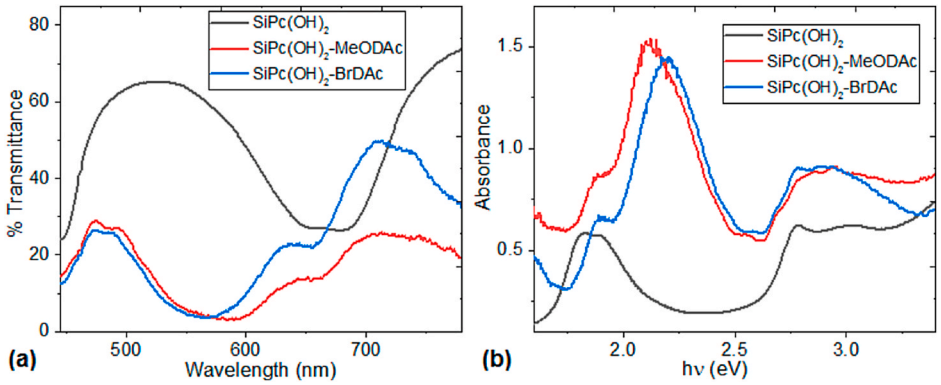

Fig. 7. (a) % Transmittance and (b) Absorbance of $SiPc(OH)_2$ and $SiPc(OH)_2$-DAc films.

Table 4
Thickness, onset gap, optical gap, and, Urbach energy for $SiPc(OH)_2$ and $SiPc(OH)_2$-DAc films.

Sample	Thickness (cm)	Indirect Onset gap (eV)	Indirect Optical gap (eV)	Direct Onset gap (eV)	Direct Optical gap (eV)	Urbach energy (eV)
$SiPc(OH)_2$	8.4×10^{-7}	2.50	3.61	–	4.39	0.2528
$SiPc(OH)_2$-MeODAc	1.59×10^{-6}	1.76	1.88	1.73	1.93	0.1546
$SiPc(OH)_2$-BrDAc	1.92×10^{-6}	1.75	1.87	1.80	1.98	0.1565

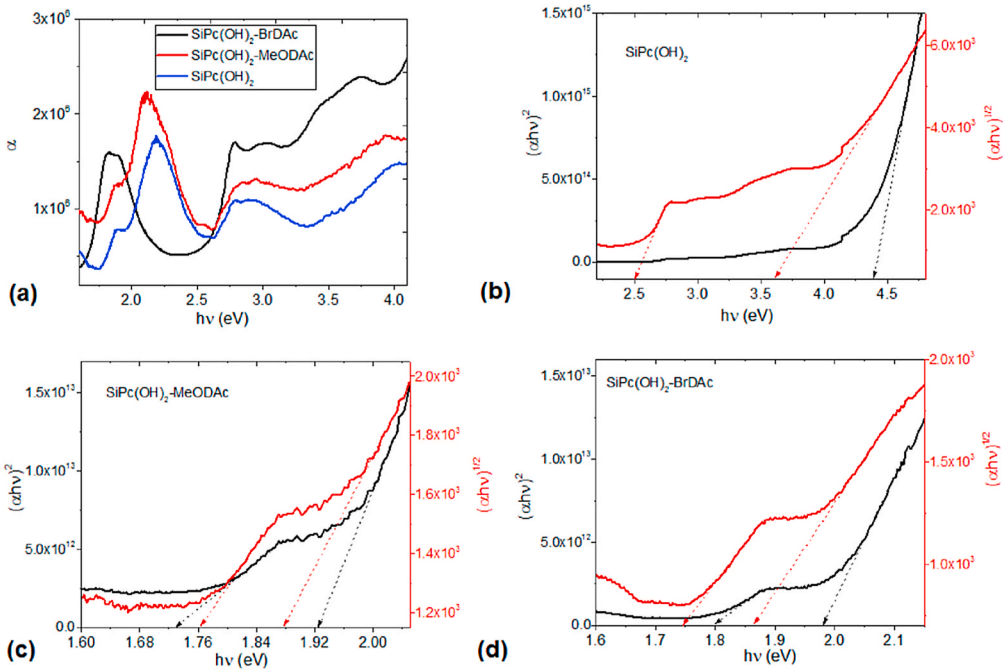

Fig. 8. (a) Absorption coefficient (α) for semiconductors films. Tauc curves for direct and indirect transitions for (b) $SiPc(OH)_2$, (c) $SiPc(OH)_2$-MeODAc and (d) $SiPc(OH)_2$-BrDAc films.

from the x-axis intercept at $(\alpha h\nu)^n = 0$, from the plot of $(\alpha h\nu)^n$ dependence with respect to $h\nu$ (Fig. 8b–d). The number n characterizes the transition process, with n = 2 and n = 1/2 for indirect and direct allowed transitions respectively [49–52]. Table 4 shows the E^{opt} obtained values for both indirect and direct transitions. It is noticed that the presence of the acid reduces both the E^{opt} and the onset gap (E^{onset}) in the films, which increases their potential as organic semiconductors. The E^{opt} value corresponds to the lower-energy transition produced by a photon absorption, and E^{onset} is ascribed to the optical absorption onset and the origin of a bound electron-hole pair, or "Frenkel exciton" [53,54]. Both values of E^{onset} and E^{opt} are shown in Fig. 8. The minimal difference between indirect and direct

band gaps values for the $SiPc(OH)_2$-DAc films arises from the substituent present within the dienynoic acids' structure. Bromide is an electronegative substituent; therefore, it behaves as an electron-withdrawer due to an inductive effect and as a weak electron-donor due to a resonant effect. The methoxy group on the other hand, is an electron-donor due to resonance (as oxygen has lone pairs that can enter the ring). The lone pair on the oxygen atom is suitably located in order to increase electron density and allow delocalization within the conjugated ring system, for better positive charge stabilization. This result is important because, if these semiconductors films are to be applied in optoelectronic or photovoltaic devices, it is relevant that the acid dopants have an electro-donating substituent in their structure. Furthermore, Table 4 shows that E^{opt} values are lower for indirect transitions, which is related to the amorphous structural arrangement of the films. This amorphous structure in the films is due to the technique used for its deposit. The thermal gradients between the powdered semiconductors and the substrates are very large, which means that when they come into contact, the semiconductor is rapidly deposited without the possibility of ordering its molecules during the formation of the film. These results match with those found by El-Damhogi et al. [44] in silicon phthalocyanine dichloride thin films. It is also noteworthy that the optical gap values both direct and indirect, obtained for $SiPc(OH)_2$-MeODAc and $SiPc(OH)_2$-BrDAc, are very similar to those reported by Vebber et al. [37] (1.80–1.82 eV) and Melville et al. [40] (1.7–1.8 eV). These optical gap values make $SiPc(OH)_2$-DAc films good candidates for use in optoelectronic devices.

To assess defects in the energy gaps, the Urbach energy (E_U) can be determined according to equation (3) [55,56]:

$$\alpha = A_a \, exp\left(\frac{h\nu}{E_U}\right) \tag{3}$$

where besides the parameters defined earlier, A_a is a material coefficient which constitutes the α at the E^{opt}. The exponential absorption edge can be explained owing to the exponential local state distribution in the bandgap [55]. Fig. 9a–c shows the linear relationship of $\ln(\alpha)$ and $h\nu$ for the films. The Urbach energy values were obtained from the reciprocal of the linear relationship slopes and recorded in Table 4. These results also coincide with those found by El-Damhogi et al. [44] in silicon phthalocyanine dichloride thin films. It is important to consider that in a perfect semiconductor the value of E_U should be zero [48]. The higher E_U belongs to the $SiPc(OH)_2$ film and the lower E_U to the $SiPc(OH)_2$-MeODAc film. Apparently, the MeODAc doped film exhibits the best semiconducting behavior with the smallest number of defects in comparison to the other films. However, the E^{onset} and E^{opt} has a values very similar to that of the SiPc $(OH)_2$-BrDAc film. This is an indication of the potential of both films to perform as active semiconductor layers in photovoltaic and optoelectronic devices.

Finally, the electrical behavior of the $SiPc(OH)_2$-DAc films was evaluated and compared, to obtain the current-voltage (I–V) relationship under diverse lighting conditions of these organic semiconductors. Fig. 1 shows the scheme of the glass/ITO/$SiPc(OH)_2$-DAc/Ag simple system manufactured for this purpose, where the $SiPc(OH)_2$-DAc film is located between the ITO and Ag electrodes. The electrical measurement was carried out in two different zones of each film, without remarkable changes in the electrical current values. The objective of this measurement was to know the charge transport of the two doped films, in order to compare the effect that each acid has on each of the semiconductor films. The undoped $SiPc(OH)_2$ film was taken as a reference or baseline, whose I–V graph is presented in Fig. 10. This is because in semiconductor materials, it is convenient to compare the electric current carried by the intrinsic or undoped semiconductor and the current carried by same semiconductor but in the doped state. With the above, the effect of the dopant can be known.

In Fig. 10, depending on the provided voltage, two different electrical conduction mechanisms can be observed. The first one, at V < 0.24 V, is ohmic behavior; the linear relationship between the I and V is observed. At V > 0.24 V, the space charge limited current (SCLC) mechanism is present. This change in behavior is due to the fact that, as the voltage increases, a circumstance is reached where the charge carriers lag behind in pace, and they accumulate in different regions of the film. The ITO/$SiPc(OH)_2$/Ag device enters the SCLC regime, which is no longer described by Ohm's law. This electrical behavior coincides with the results obtained by El-Damhogi et al. [57] for $SiPc(Cl)_2$ films, where silicon appears with the same coordination state, and the substituents tend to present the same type of behavior in the phthalocyanine molecule. On the other hand, in Fig. 10 it is observed that the intrinsic $SiPc(OH)_2$ film is not affected by the different lighting conditions. The only difference is in its behavior in dark conditions, where although the current transported is lower in the range dominated by SCLC, at higher voltages it continues to rise, while in lighting conditions it remains constant.

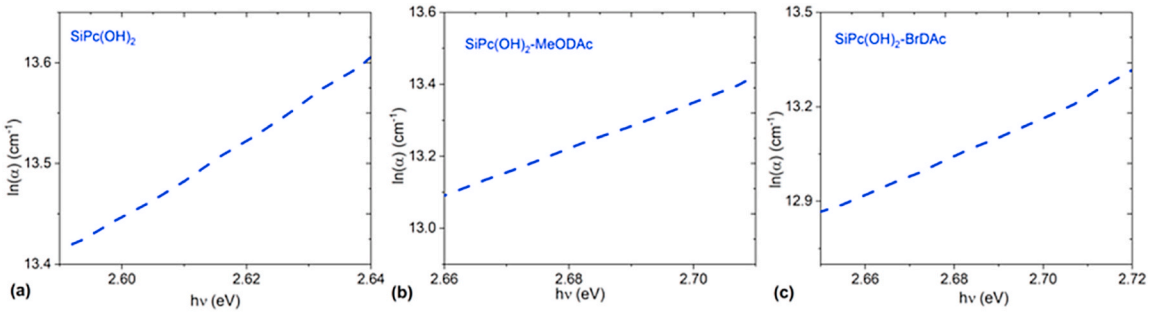

Fig. 9. Plot of ln (α) vs. hυ for (a) $SiPc(OH)_2$, (b) $SiPc(OH)_2$-MeODAc and (c) $SiPc(OH)_2$-BrDAc films.

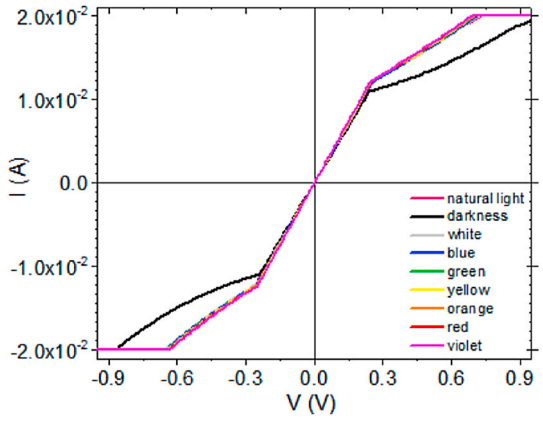

Fig. 10. I–V characteristic of ITO/SiPc$(OH)_2$/Ag at different lighting conditions in forward and reverse bias.

In Fig. 11a-b it can be seen that ITO/SiPc$(OH)_2$-DAc/Ag, exhibit mostly an ambipolar behavior, which is more evident in the SiPc$(OH)_2$-MeODAc film (Fig. 11b), which also allows the greatest flow of electrical current. It is noticeable that although the carried current is lower in our case, the type of behavior is similar to that found by El-Damhogi et al. [57]. This type of behavior presented by the SiPc$(OH)_2$-MeODAc films is also presented in other MPcs films such as: that obtained for MnPc films doped with iodide [58], CuPc films [59] or AlPcCl [60]. This ambipolar behavior it is an interesting result, since the injection of charges, holes, or electrons is generated similarly, regardless of whether the ITO and Ag have an anode or cathode function. In the *I–V* graphs of Fig. 11, it is also observed that at low voltages (<0.3V for SiPc$(OH)_2$-MeODAc and <0.4V for SiPc$(OH)_2$-BrDAc), the incident radiation upon the devices produces no significant effect on charge transport. It was observed that at high voltages the effect becomes more significant, and for the device, with SiPc$(OH)_2$-BrDAc the highest current carrying occurs in front of white radiation (9.21×10^{-9} A) and later in dark conditions (6.37×10^{-9} A), whereas for the device with SiPc$(OH)_2$-MeODAc, the highest current of 5.68×10^{-5} A is generated with natural lighting, and again followed by the current in dark conditions (4.17×10^{-5} A). This type of behavior may be appropriate in active layers that are part of electronic or photovoltaic devices with transparent substrate and anode, in which the effect of some types of radiation can enhance charge transport in the devices. According to the schematic energy diagram illustrated in Fig. 11c–d and which takes the values of HOMO and LUMO from Table 2, when the external voltage is applied onto the device electrodes, from the ITO with a work function (φ) of 4.7 eV, holes were injected into the HOMO of SiPc$(OH)_2$-DAc, while from Ag with $\varphi = 4.2$ eV, the injection of electrons takes place towards the LUMO of SiPc$(OH)_2$-DAc. The charge carriers move along the phthalocyanine and the acid until, induced by Coulomb attraction, electrons and holes meet, giving place to the electron-hole pair or exciton that recombines more efficiently in the device with SiPc$(OH)_2$-MeODAc film. It is also important to consider that this device presents changes in the slope of the curves obtained under natural lighting and in dark conditions, at 0.65 V and 0.85 V respectively. These changes in slope are caused by variations in the electrical behavior of the device: at low voltages its ohmic behavior, while at high voltages, a saturation of charges is generated in certain regions of the film, resulting in SCLC behavior. Definitely, the presence of the dienynoic acid affects the electrical behavior of the SiPc$(OH)_2$-DAc films. In this work, the SiPc$(OH)_2$-MeODAc film carries the largest amount of electric current (4.17×10^{-5} A) in darkness, and this maximum value is in the same order of magnitude as for the InPcCl film (2×10^{-5} A) [61], and an order of magnitude lower than CuPc (1.5×10^{-4}) [59]. The maximum current transported for SiPc$(OH)_2$-MeODAc is also higher: it is an order of magnitude greater than those derived from ZnPc (2.2×10^{-6} A) and TiOPc (1.8×10^{-6} A) [62] and two orders of magnitude greater than MnPc (1×10^{-7} A) [58]. However, it is worthy of mention that, although the inclusion of the dopant in the phthalocyanine presents advantages, it also presents an important disadvantage: the maximum current of the device is several orders of magnitude smaller than the one with the undoped SiPc$(OH)_2$ film (see Fig. 10). These results of films based on SiPc$(OH)_2$, give the potential to continue studying them in the future, with other dopants, and as active layers in optoelectronic devices.

5. Conclusions

Actives layers constituted by SiPc$(OH)_2$ doped with (2E, 4Z)-5, 7-diphenylhepta-2, 4-dien-6-ynoic acids (DAc) were deposited. The good agreement between experimental and simulated IR spectra confirmed that the theoretical calculations accurately reproduce simulated and experimental band positions of SiPc$(OH)_2$-DAc. A molecular orbital and theoretical energy gap analyses were carried out and additionally, the experimental optical gap, onset gap and Urbach energy, were obtained from a UV–vis spectral study of the absorption dependence near the fundamental absorption edges. The band gaps for direct and indirect electronic transitions were determined; however, indirect transitions are predominant owing to the amorphous structural composition of the films. The SiPc$(OH)_2$-MeODAc film has an indirect optical gap of 1.88 eV and a onset gap of 1.76 eV, while the SiPc$(OH)_2$-BrDAc film has an optical and onset gap of 1.87 eV and 1.75 eV respectively. The optical behavior in films is influence by the type of dienynoic acid. Additionally, a low Urbach energy of 0.15 eV was obtained, which is an indicator of a low number of film defects. In other hand, two glass/ITO/SiPc$(OH)_2$-DAc/Ag systems were manufactured, and their electrical behavior was assessed under different lighting conditions. These results were compared to the undoped phthalocyanine device. The measurements exhibited symmetrical behavior which revealed the

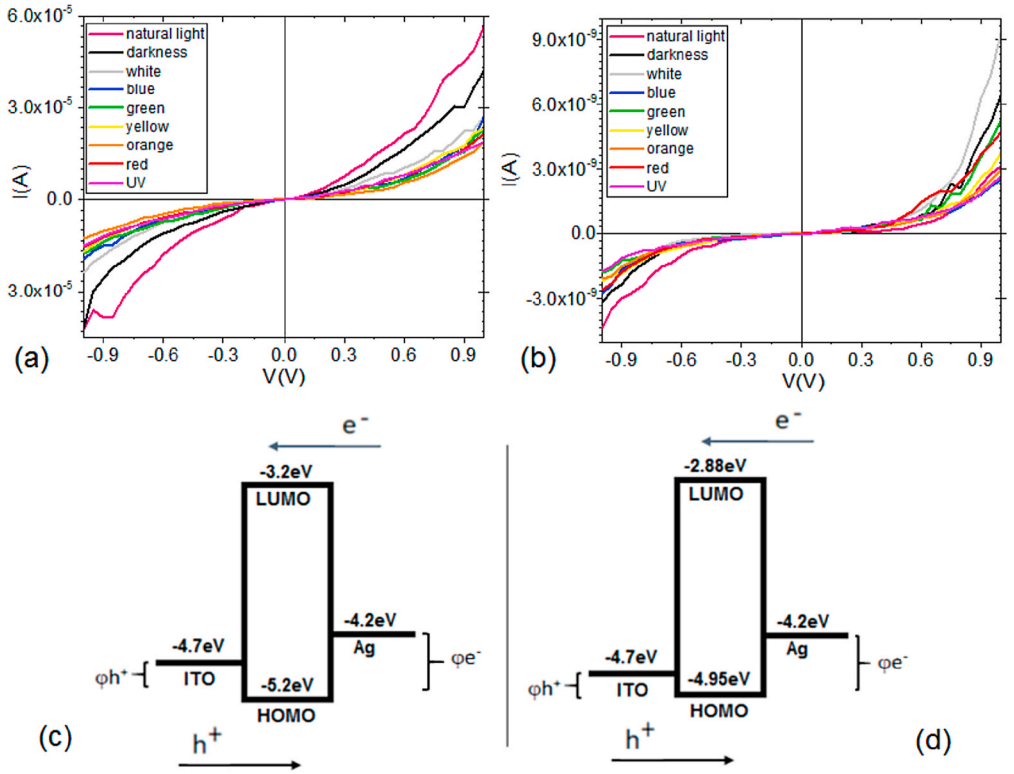

Fig. 11. I–V curves for different lighting conditions of glass/ITO/SiPc(OH)$_2$-DAc/Ag with (a) SiPc(OH)$_2$-MeODAc and (b) SiPc(OH)$_2$-BrDAc films. Schematic energy diagram of devices with (c) SiPc(OH)$_2$-MeODAc and (d) SiPc(OH)$_2$-BrDAc. The values of HOMO and LUMO were taken from Table 2.

ambipolarity of SiPc(OH)$_2$-DAc as an active layer, and the dependence between transported I and V under incident lighting conditions. However, the presence of the dienynoic acid affects the electrical behavior of the semiconductor films in the devices. The SiPc(OH)$_2$-MeODAc film reaches a maximum current of 5.68 $\times$ 10^{-5} A for natural light condition, while the SiPc(OH)$_2$-BrDAc film, reaches a maximum current of 9.21 $\times$ 10^{-9} A for white illumination condition. However, these maximum current are several orders of magnitude smaller than in the undoped SiPc(OH)$_2$ film device. Although in terms of the optical behavior, dienynoic acids have a positive effect on semiconductor films, in terms of electrical properties, their presence decreases the transport of charge carriers.

Data availability

Data will be made available on request.

CRediT authorship contribution statement

María Elena Sánchez Vergara: Writing – review & editing, Writing – original draft, Validation, Supervision, Project administration, Methodology, Funding acquisition, Formal analysis, Data curation, Conceptualization. **Emilio I. Sandoval Plata:** Writing – review & editing, Writing – original draft, Methodology, Investigation, Formal analysis, Data curation. **Ricardo Ballinas Indili:** Writing – review & editing, Writing – original draft, Visualization, Validation, Methodology, Formal analysis. **Roberto Salcedo:** Writing – review & editing, Writing – original draft, Validation, Software, Resources, Methodology, Formal analysis, Data curation, Conceptualization. **Cecilio Álvarez Toledano:** Writing – review & editing, Writing – original draft, Validation, Supervision, Resources, Project administration, Funding acquisition.

Declaration of competing interest

The authors declare that they have no known competing financial interests or personal relationships that could have appeared to influence the work reported in this paper.

Acknowledgments

The authors wish to express their gratitude to M. in Eng. Citlalli Rios for technical help and English revision. María Elena Sánchez Vergara thanks the COMECYT, FICDTEM-2023-65. Cecilio Álvarez Toledano gratefully acknowledges the financial support DGAPA-PAPIIT Project Number IN213523.

References

[1] P.P. Manousiadis, K. Yoshida, G.A. Turnbull, I.D.W. Samuel, Organic semiconductors for visible light communications, Phil. Trans. R. Soc. A378 (2020) 2169, https://doi.org/10.1098/rsta.2019.0186.
[2] C.R. Newman, C.D. Frisbie, D.A. da Silva Filho, J.-L. Brédas, P.C. Ewbank, K.R. Mann, Introduction to organic thin film transistors and design of n-channel organic semiconductors, Chem. Mater. 16 (23) (2004) 4436–4451, https://doi.org/10.1021/cm049391x.
[3] L. Dou, Y. Liu, Z. Hong, G. Li, Y. Yang, Low-bandgap near-IR conjugated polymers/molecules for organic electronics, Chem. Rev. 115 (23) (2015) 12633–12665, https://doi.org/10.1021/acs.chemrev.5b00165.
[4] I. Salzmann, G. Heimel, M. Oehzelt, S. Winkler, N. Koch, Molecular electrical doping of organic semiconductors: fundamental mechanisms and emerging dopant design rules, Acc. Chem. Res. 49 (3) (2016) 370–378, https://doi.org/10.1021/acs.accounts.5b00438.
[5] B. Neil, McKeown, Phthalocyanine Materials: Synthesis, Structure and Function, first ed., Cambridge University Press, 1998, 0-521-49623-3.
[6] T. Torres, From subphthalocyanines to subporphyrins, Angew. Chem. Int. Ed. 45 (18) (2006) 2834–2837, https://doi.org/10.1002/anie.200504265.
[7] C.A. Barker, K.S. Findlay, S. Bettington, A.S. Batsanov, I.F. Perepichka, M.R. Bryce, A. Beeby, Synthesis of new axially-disubstituted silicon-phthalocyanine derivatives: optical and structural characterization, Tetrahedron 62 (40) (2006) 9433–9439, https://doi.org/10.1016/j.tet.2006.07.046.
[8] C.G. Claessens, U.W.E. Hahn, T. Torres, Phthalocyanines: from outstanding electronic properties to emerging applications, Chem. Rec. 8 (2) (2008) 75–97, https://doi.org/10.1002/tcr.20139.
[9] K. Mitra, M.C. Hartman, Silicon phthalocyanines: synthesis and resurgent applications, Org, Biomol. Chem. 19 (6) (2021) 1168–1190, https://doi.org/10.1039/D0OB02299C.
[10] A.K. Pal, S. Varghese, D.B. Cordes, A.M.Z. Slawin, I.D.W. Samuel, E. Zysman-Colman, Near-Infrared fluorescence of silicon phthalocyanine carboxylate esters, Sci. Rep. 7 (2017) 12282, https://doi.org/10.1038/s41598-017-12374-8.
[11] M. Abd-El Salam, H.M. El-Mallah, D.G. El-Damhogi, E. Elesh, Thermal analysis, dielectric response and electrical conductivity of silicon phthalocyanine dichloride ($SiPcCl_2$) thin films, J. Electron. Mater. 50 (2) (2021) 562–570, https://doi.org/10.1007/s11664-020-08604-x.
[12] P. Atkins, T. Overton, J. Rourke, M. Weller, D.F. Shriver, F. Armstrong, Inorganic Chemistry, fifth ed., Oxford University Press, 2010, 978-0-19-923617-6.
[13] R.D. Joyner, M.E. Kenney, Phthalocyaninosilicon compounds, Inorg. Chem. 1 (2) (1962) 236–238, https://doi.org/10.1021/ic50002a008.
[14] B.H. Lessard, The rise of silicon phthalocyanine: from organic photovoltaics to organic thin film transistors, ACS Appl. Mater. Interfaces 13 (2021) 31321–31330, https://doi.org/10.1021/acsami.1c06060.
[15] T.M. Grant, D.S. Josey, K.L. Sampson, T. Mudigonda, T.P. Bender, B.H. Lessard, Boron subphthalocyanines and silicon phthalocyanines for use as active materials in organic photovoltaics, Chem. Rec. 19 (2019) 1093–1112, https://doi.org/10.1002/tcr.201800178.
[16] H. Lu, N. Kobayashi, Optically active porphyrin and phthalocyanine systems, Chem. Rev. 116 (2016) 6184–6261, https://doi.org/10.1021/acs.chemrev.5b00588.
[17] M.K. Lowery, A.J. Starshak, J.N. Esposito, P.C. Krueger, M.E. Kenney, Dichloro(Phthalocyanino)silicon, Inorg. Chem. 4 (1965) 128, https://doi.org/10.1021/ic50023a036.
[18] Ch Zhong, Y. Yan, Q. Peng, Z. Zhang, T. Wang, X. Chen, J. Wang, Y. Wei, T. Yang, L. Xie, Structure–property relationship of macrocycles in organic photoelectric devices: a comprehensive review, Nanomaterials 13 (2023) 1750, https://doi.org/10.3390/nano13111750.
[19] R. Ballinas-Indili, M.E. Sánchez-Vergara, R.A. Toscano, C. Álvarez-Toledano, Synthesis, doping and characterization of new molecular semiconductors containing (2E, 4z)-5, 7-diphenylhepta-2, 4-dien-6-ynoic acids, J. Inorg. Organomet. Polym. 30 (2020) 2509–2519, https://doi.org/10.1007/s10904-019-01430-7.
[20] A.D. Becke, Density-functional exchange-energy approximation with correct asymptotic behavior, Phys. Rev. A 38 (1988) 3098–3100, https://doi.org/10.1103/PhysRevA.38.3098.
[21] J.P. Perdew, Y. Wang, Accurate and simple analytic representation of the electron-gas correlation energy, Phys. Rev. B 45 (1992) 13244–13249, https://doi.org/10.1103/PhysRevB.45.13244.
[22] M.J. Frisch, G.W. Trucks, H.B. Schlegel, G.E. Scuseria, M.A. Robb, J.R. Cheeseman, G. Scalmani, V. Barone, G.A. Petersson, H. Nakatsuji, X. Caricato, M. Li, A. V. Marenich, J. Bloino, B.G. Janesko, R. Gomperts, B. Mennucci, H.P. Hratchian, J. Ortiz, A.F. Izmaylov, J.L. Sonnenberg, D. Williams-Young, F. Ding, F. Lipparini, f Egidi, J. Goings, B. Peng, A. Petrone, T. Henderson, D. Ranasinghe, V.G. Zakrzewski, J. Gao, N. Rega, G. Zheng, W. Liang, M. Hada, M. Ehara, K. Toyota, R. Fukuda, J. Hasegawa, M. Ishida, T. Nakajima, Y. Honda, O. Kitao, H. Nakai, T. Vreven, K. Throssell, J.A. Montgomery, J.E. Peralta, F. Ogliaro, M. J. Bearpark, J.J. Heyd, E.N. Brothers, K.N. Kudin, V.N. Staroverov, T.A. Keith, R. Kobayashi, J. Normand, K. Raghavachari, A.P. Rendell, J.C. Burant, S. S. Iyengar, J. Tomasi, M. Cossi, J.M. Millam, C. Klene Adamo, R. Cammi, J.W. Ochterski, R.L. Martin, K. Morokuma, O. Farkas, J.B. Foresman, D.J. Fox, Gaussian, Inc., Wallingford CT, 2016.
[23] Y. Zhao, D.G. Truhlar, A new local density functional for main-group thermochemistry, transition metal bonding, thermochemical kinetics, and noncovalent interactions, J. Chem. Phys. 125 (19) (2006) 194101, https://doi.org/10.1063/1.2370993.
[24] R.K. Raju, A.A. Bengali, E.N. Brothers, A unified set of experimental organometallic data used to evaluate modern theoretical methods, Dalton Trans. 45 (2016) 13766–13778, https://doi.org/10.1039/C6DT02763F.
[25] E.D. Glowascki, M. Irimia-Vladu, S. Baur, N.S. Sariciftci, Hydrogen-bonds in molecular solids-from biological systems to organic electronics, J. Mater. Chem. B 1 (2013) 3742–3753, https://doi.org/10.1039/C3TB20193G.
[26] D.G. Solgun, A.A. Tanriverdi, U. Yildiko, M.S. Ağirtaş, Synthesis of axially silicon phthalocyanine substituted with bis-(3,4-dimethoxyphenethoxy) groups, DFT and molecular docking studies, J. Inclusion Phenom. Macrocycl. Chem. 102 (2022) 851–860, https://doi.org/10.1007/s10847-022-01164-z.
[27] A. Karakas, Y. Ceylan, M. Karakaya, M. Taser, B.B. Terlemez, N. Eren, Y. El Kouari, M. Lougdali, A.K. Arof, B. Sahraoui, Theoretical diagnostics of second and third order hyperpolarizabilities of several acid derivatives, Journal Open Chemistry 17 (2019) 151–156, https://doi.org/10.1515/chem-2019-0020.
[28] Y.-J. Cheng, S.-H. Yang, C.-S. Hsu, Synthesis of conjugated polymers for organic solar cell applications, Chem. Rev. 109 (11) (2009) 5868–5923, https://doi.org/10.1021/cr900182s.
[29] R. Seoudi, G.S. El-Bahy, Z.A. El-Sayed, FTIR, TGA and DC electrical conductivity studies of phthalocyanine and its complexes, J. Mol. Struct. 753 (1–3) (2005) 119–126, https://doi.org/10.1016/j.molstruc.2005.06.003.
[30] A. Rodríguez-Gómez, C.M. Sánchez-Hernández, I. Fleitman-Levin, J. Arenas-Alatorre, J.C. Alonso-Huitrón, M.E. Sánchez-Vergara, Optical absorption and visible photoluminescence from thin films of silicon phthalocyanine derivatives, Materials 7 (9) (2014) 6585–6603, https://doi.org/10.3390/ma7096585.
[31] N. Touka, H. Benelmadjat, B. Boudine, O. Halimi, M. Sebais, Copper phthalocyanine nanocrystals embedded into polymer host: preparation and structural characterization, J. Assoc. Arab Univ. Basic Appl. Sci. 13 (1) (2013) 52–56, https://doi.org/10.1016/j.jaubas.2012.03.002.
[32] M.M. El-Nahass, K.F. Abd-El-Rahman, A.A. Al-Ghamdi, A.M. Asiri, Optical properties of thermally evaporated tin-phthalocyanine dichloride thin films, $SnPcCl_2$, Phys. B Condens. Matter. 344 (1–4) (2014) 398–406, https://doi.org/10.1016/j.physb.2003.10.019.
[33] M.M. El-Nahass, A.M. Farag, K.F. Abd-El-Rahman, A.A.A. Darwish, Dispersion studies and electronic transitions in nickel phthalocyanine thin films, Opt Laser. Technol. 37 (7) (2005) 513–523, https://doi.org/10.1016/j.optlastec.2004.08.016.

[34] R.R. Cranston, B.H. Lessard, Metal phthalocyanines: thin-film formation, microstructure, and physical properties, RSC Adv. 11 (35) (2021) 21716–21737, https://doi.org/10.1039/D1RA03853B.

[35] A.A.A. Darwish, S. Helali, S.I. Qashou, I.S. Yahia, E.F.M. El-Zaidia, Studying the surface morphology, linear and nonlinear optical properties of manganese (III) phthalocyanine chloride/FTO films, Phys. B Condens. Matter 622 (2021) 413355, https://doi.org/10.1016/j.physb.2021.413355.

[36] M. Özçeşmeci, I. Nar, E. Hamuryudan, Synthesis and electrochemical and spectroelectrochemical characterization of chloromanganese(III) phthalocyanines, Turk. J. Chem. 38 (6) (2014) 1064–1072, https://doi.org/10.3906/kim-1405-43.

[37] M.C. Vebber, T.M. Grant, J.L. Brusso, B.H. Lessard, Bis(trialkylsilyl oxide) silicon phthalocyanines: understanding the role of solubility in device performance as ternary additives in organic photovoltaics, Langmuir 36 (2020) 2612–2621, https://doi.org/10.1021/acs.langmuir.9b03772.

[38] S. Honda, H. Ohkita, H. Benten, S. Ito, Multi-colored dye sensitization of polymer/fullerene bulk heterojunction solar cells, Chem. Commun. 46 (2010) 6596–6598, https://doi.org/10.1039/c0cc01787f.

[39] T.M. Grant, Ch Dindault, N.A. Rice, S. Swaraj, B.H. Lessard, Synthetically facile organic solar cells with 44% efficiency using P3HT and a silicon phthalocyanine non-fullerene acceptor, Mater. Adv. 2 (2021) 2594–2599, https://doi.org/10.1039/d1ma00165e.

[40] O.A. Melville, T.M. Grant, K. Lochhead, B. King, R. Ambrose, N.A. Rice, N.T. Boileau, A.J. Peltekoff, M. Tousignant, I.G. Hill, B.H. Lessard, Contact engineering using manganese, chromium, and bathocuproine in group 14 phthalocyanine organic thin-film transistors, ACS Appl. Electron. Mater. 2 (2020) 1313–1322, https://doi.org/10.1021/acsaelm.0c00104.

[41] M. Polyakov, V. Ivanova, D. Klyamer, B. Köksoy, A. Senocak, E. Demirba, M. Durmu, T. Basova, A hybrid nanomaterial based on single walled carbon nanotubes cross-linked via axially substituted silicon (IV) phthalocyanine for chemiresistive sensors, Molecules 25 (2020) 2073, https://doi.org/10.3390/molecules25092073.

[42] K.P. Madhuri, N.S. John, S. Angappane, P.K. Santra, F. Bertram, Influence of iodine doping on the structure, morphology, and physical properties of manganese phthalocyanine thin films, J. Phys. Chem. C 122 (2018) 28075–28084, https://doi.org/10.1021/acs.jpcc.8b08205.

[43] Al-Ghamdi, T. Hamdalla, A.A.A. Darwish, S.A.A.O.M. Alzahrani, E.F.M. El-Zaidia, N.A. Alamrani, M.A. Elblbesy, I.S. Yahia, Preparation, Raman spectroscopy, surface morphology and optical properties of $TiPcCl_2$ nanostructured films: thickness effect, Opt. Quant. Electron. 53 (2021) 514, https://doi.org/10.1007/s11082-021-03163-9.

[44] D.G. El-Damhogi, H.M. El-Mallah, M.A. El-Salam, E. Elesh, UV- irradiation induced changes in structural and optical characterization of silicon phthalocyanine dichloride (SiPcCl2) thin films, Silicon 13 (2021) 4601–4609, https://doi.org/10.1007/s12633-020-00778-7.

[45] J. Sharp, M. Abkowitz, Dimeric structure of a copper phthalocyanine polymorph, J. Phys. Chem. A 77 (1973) 477–481, https://doi.org/10.1021/j100623a012.

[46] M. El-Nahass, K. Abd-El-Rahman, A. Darwish, Fourier transform infrared and UV–vis spectroscopes of nickel phthalocyanine thin films, Mater. Chem. Phys. 92 (2005) 185–189, https://doi.org/10.1016/j.matchemphys.2005.01.008.

[47] M. Makhlouf, A. El-Denglawey, H. Zeyada, M. El-Nahass, The structural and optical characterizations of tetraphenylporphyrin thin films, J. Lumin. 147 (2014) 202–208, https://doi.org/10.1016/j.jlumin.2013.11.007.

[48] T. Fazal, S. Iqbal, M. Shah, B. Ismail, N. Shaheen, H. Alrbyawi, M.M. Al-Anazy, E.B. Elkaeed, H.H. Somaily, R.A. Pashameah, E. Alzahrani, A.-E. Farouk, Improvement in optoelectronic properties of bismuth sulphide thin films by chromium incorporation at the orthorhombic crystal lattice for photovoltaic applications, Molecules 27 (2022) 6419, https://doi.org/10.3390/molecules27196419.

[49] J. Tauc, Optical properties and electronic structure of amorphous Ge and Si, Mater. Res. Bull. 3 (2) (1968) 37–46, https://doi.org/10.1016/0025-5408(68)90023-8.

[50] N. Laidani, R. Bartali, G. Gottardi, M. Anderle, P. Cheyssac, Optical absorption parameters of amorphous carbon films from forouhi-bloomer and tauc-lorentz models: a comparative study, J. Phys. Condens. Matter 20 (1) (2008) 015216, https://doi.org/10.1088/0953-8984/20/01/015216.

[51] T.M. Mok, S.K. O'Leary, The dependence of the Tauc and Cody optical gaps associated with hydrogenated amorphous silicon on the film thickness: αl Experimental limitations and the impact of curvature in the Tauc and Cody plots, J. Appl. Phys. 102 (11) (2007) 113525, https://doi.org/10.1063/1.2817822.

[52] M. Dongol, M.M. El-Nahass, A. El-Denglawey, A.F. Elhady, A.A. Abuelwafa, Optical properties of nano 5,10,15,20-tetraphenyl-21H,23H-porphyrin nickel (II) thin film, Curr. Appl. Phys. 12 (4) (2012) 1178–1184, https://doi.org/10.1016/j.cap.2012.02.051.

[53] A.A. Al-Muntaser, M.M. El-Nahass, A.H. Oraby, M.S. Meikhail, H.M. Zeyada, Structural and optical characterization of thermally evaporated nanocrystalline 5,10,15,20-tetraphenyl-21H,23H-porphine manganese (III) chloride thin films, Optik 167 (2018) 204–217, https://doi.org/10.1016/j.ijleo.2018.04.041.

[54] E.V. Tsiper, Z.G. Soos, W. Gao, A. Kahn, Electronic polarization at surfaces and thin films or organic molecular crystals: PTCDA, Chem. Phys. Lett. 360 (1–2) (2002) 47–52, https://doi.org/10.1016/S0009-2614(02)00774-1.

[55] S.A. Al-Ghamdi, T.A. Hamdalla, A.A.A. Darwish, A.O.M. Alzahrani, E.F.M. El-Zaidia, N.A. Alamrani, M.A. Elblbesy, I.S. Yahia, Preparation, Raman spectroscopy, surface morphology and optical properties of $TiPcCl_2$ nanostructured films: thickness effect, Opt. Quant. Electron. 53 (2021) 514, https://doi.org/10.1007/s11082-021-03163-9.

[56] M.G. Ghanem, Y. Badr, T.A. Hameed, M.E. Marssi, A. Lahmar, H.A. Wahab, I.K. Battisha, Synthesis and characterization of undoped and Er-doped ZnO nanostructure thin films deposited by sol-gel spin coating technique, Mater. Res. Express 6 (8) (2019) 085916, https://doi.org/10.1088/2053-1591/ab2750.

[57] D.G. El-Damhogi, H.M. El-Mallah, M.A. El-Salam, E. Elesh, Fabrication, carrier transport mechanisms and photovoltaic properties of Au/silicon phthalocyanine dichloride/p-Si/Al heterojunction device, Opt. Quant. Electron. 52 (2020) 429, https://doi.org/10.1007/s11082-020-02546-8.

[58] K.P. Madhuri, N.S. John, S. Angappane, P.K. Santra, F. Bertram, Influence of iodine doping on the structure, morphology, and physical properties of manganese phthalocyanine thin films, J. Phys. Chem. C 122 (2018) 28075–28084, https://doi.org/10.1021/acs.jpcc.8b08205.

[59] Z. Ahmad, M.H. Sayyad, KhS. Karimov, CuPc based organic-inorganic hetero-junction with Au electrodes, J. Semiconduct. 31 (7) (2010), https://doi.org/10.1088/1674-4926/31/7/074002, 074002-1 074002-4.

[60] I.M. Soliman, M.M. El-Nahass, B.A. Khalifa, Characterization and photovoltaic performance of organic device based on AlPcCl/p-Si heterojunction, Synth. Met. 209 (2015) 55–59, https://doi.org/10.1016/j.synthmet.2015.06.016.

[61] H.M. Zeyada, M.M. El-Nahass, E.M. El-Menyawy, A.S. El-Sawah, Electrical and photovoltaic characteristics of indium phthalocyanine chloride/p-Si solar cell, Synth. Met. 207 (2015) 46–53, https://doi.org/10.1016/j.synthmet.2015.06.008.

[62] D.V. Bonegardt, D.D. Klyamer, D. Atilla, A. Gül Gürek, T.V. Basova, Thin films of poly(oxyethylene)-substituted phthalocyaninato zinc(II) and oxotitanium(IV) complexes: synthesis, structure and sensor response to ammonia, J. Mater. Sci. Mater. Electron. 32 (2021) 5955–5964, https://doi.org/10.1007/s10854-021-05316-8.